GEOPHYSICS. VOL. 76, NO. 6 (NOVEMBER-DECEMBER 2011); P. N55–N64, 8 FIGS., 2 TABLES.
10.1190/GEO2010-0169.1

Differential form and numerical implementation of Biot's poroelasticity equations with squirt dissipation

José M. Carcione[1] and Boris Gurevich[2]

ABSTRACT

The squirt-flow wave attenuation mechanism is implemented in Biot's theory of poroelasticity in the form of differential equations. All the stiffnesses involved in the stress-strain relation become complex and frequency dependent, which can exactly be expressed in terms of kernels based on the Zener mechanical model. In the time domain, this approach implies time convolutions, which are circumvented by introducing memory variables. The differential equations are consistent with Gassmann's and Mavko-Jizba equations at low and high frequencies, respectively. All the coefficients in the poro-viscoelastic differential equations have a clear physical meaning and can be obtained or estimated from independent measurements. The key additional parameters are the dry-rock bulk modulus at a confining pressure where all the compliant pores are closed, i.e., a hypothetical rock without the soft porosity, the grain-contact aspect ratio and the compliant porosity. We recasted the wave equation in the particle-velocity/stress formulation and solved it by using a time-splitting technique and the Fourier pseudospectral method to compute the spatial derivatives. The algorithm can be used to obtain synthetic wave fields in inhomogeneous media.

INTRODUCTION

The theory of poroelasticity is widely used today in many geophysical applications. The most versatile approach was developed by Biot in the 1950s (Biot, 1962; Carcione, 2007; Chapter 7), who obtained the dynamical equations for wave propagation in a fully saturated medium. The theory assumes that the anelastic effects arise from viscous interaction between the fluid and the solid, and predicts two P-waves and one S-wave. Basically, the fast P-wave has solid and fluid motions in phase, and the slow (Biot) P-wave has out of phase motions. At low frequencies, the slow wave becomes diffusive because the fluid viscosity effects dominate over the inertial effects. At high frequencies, the inertial effects are predominant and the Biot mode may behave as a wave under certain conditions, which depend on the amount of clay and permeability (Klimentos, 1988).

Although Biot's theory is widely used to model the behavior of porous media, it is known to underestimate attenuation of fast P- and S-waves. The only attenuation mechanism obtained from the dispersion equation of Biot's theory is the so-called global flow, that is, wavelength-scale equilibration between the peaks and troughs of the wave. For typical rocks, the characteristic frequency of this mechanism is on the order of tens of kHz or higher. Another mechanism that can be modeled using Biot's theory is associated with mesoscopic flow between areas of different compliance within the rock (White et al., 1976; Gurevich and Lopatnikov, 1995; Pride et al., 2004; Müller et al., 2010). The word "mesoscopic" refers to the size of inhomogeneities being much larger than the typical grain size but much smaller than the wavelength of the pulse. For instance, if there are mesoscopic patches of gas in a brine-saturated sandstone, diffusion of pore fluid between the patches dissipates the energy through conversion into the diffusive slow mode (White, 1975; Norris, 1993; Johnson, 2001; Toms et al., 2006). The mesoscopic flow mechanism can be modeled using Biot's equations of poroelasticity with spatially varying coefficients (e.g., Rubino et al., 2007; Masson and Pride, 2007). However, in field-scale seismic numerical modeling it is often more efficient to approximate the corresponding relaxation peak with a Zener (1948) viscoelastic model (e.g., Carcione et al., 2006).

Another important loss mechanism at high frequencies is the so-called "squirt flow," by which there is flow from fluid-filled microcracks (grain contacts) to the pore space and vice versa (Mavko and Nur, 1975; O'Connell and Budiansky, 1977; Jones, 1986). Biot (1962) was the first to discuss this mechanism and propose a viscoelastic mechanical model to describe it. Quoting Biot:

Manuscript received by the Editor 1 June 2010; revised manuscript received 16 May 2011; published online 22 December 2011.
[1]Istituto Nazionale di Oceanografia e di Geofisica Sperimentale (OGS), Trieste, Italy. E-mail: jcarcione@inogs.it.
[2]Geophysics, Curtin University, Perth, Australia. E-mail: B.Gurevich@curtin.edu.au

"When two elastic bodies are in contact and are surrounded by a viscous fluid, a force applied in a direction normal to the area of contact will tend to squeeze the flow away from this area. Because of fluid viscosity, the fluid will not move away instantaneously. A time delay, which is exemplified by the equivalent spring dashpot model of Figure 4, will be involved." Using Biot's notation, this model is given by

$$\kappa^* = \kappa_0 + \frac{\kappa_1 r}{i\omega + r}, \tag{1}$$

where κ^* is the (drained) compressibility, κ_0, κ_1, and r are constants, and ω is the angular frequency. It can easily be shown that this model corresponds to a dry-rock bulk modulus $K = 1/\kappa^*$ given by a Zener model (e.g., Carcione, 2007) with relaxation times $\tau_\epsilon = 1/r$ and $\tau_\sigma = 1/[r(1 + \kappa_1/\kappa_0)]$, and relaxed modulus $M_R = 1/(\kappa_0 + \kappa_1)$.

The problem resides in finding a suitable squirt-flow model, in which the Zener parameters can be entirely estimated from the microstructural properties of the rock. Such a model has recently been proposed by Gurevich, et al., (2009, 2010). To include the squirt mechanism in a poroelastic numerical algorithm, one needs to replace the coefficients of the equations of poroelasticity with time-domain integro-differential operators corresponding to the solution of a dispersion equation of that mechanism. The problem is that most mathematical models of squirt flow are very complicated and corresponding dispersion equations often contain special functions of frequency that do not lend themselves to explicit representation in time domain (Murphy, 1986; Chapman et al., 2002; Pride et al., 2004). However, Gurevich et al. (2010) propose a simple squirt-flow model in which the dispersion equation corresponds directly with the Zener viscoelastic model. This is important because this model can be expressed in the time domain by using memory variables (Carcione, 1998; Carcione and Helle, 1999; Arntsen and Carcione, 2001; Carcione et al., 2006; Carcione, 2007).

The expression for the peak frequency of the relaxation mechanism is similar to the usual expression (e.g., Jones, 1986), except that in the present model, the bulk modulus of the rock is replaced by a combination of bulk and shear moduli. For liquid-saturated rocks the attenuation and dispersion curves are symmetric about the characteristic frequency in a log-log scale, consistent with the Zener model. The dissipation factor is proportional and inversely proportional to the frequency at the low- and high-frequency ranges, respectively, and the magnitude of attenuation and dispersion is directly related to the variation of the dry-rock bulk modulus with pressure. All these features are characteristic of the double-porosity model of Pride et al. (2004), but the present model is based on a different theoretical approach and is much simpler to implement. The parameters can be measured or estimated from measurements of ultrasonic velocities and strains versus confining pressure on dry samples. The workflow for estimation of these parameters is described in Gurevich et al. (2010). One assumption in this workflow is that all compliant pores are closed at the upper limit of the pressure range of the measurements and hence ultrasonic velocities become independent of pressure. Therefore, there is no squirt at these pressures and the saturated and dry velocities should approximately satisfy Gassmann's (or Biot) equations.

The experimental validation of the model requires a comparison of its predictions against measurements of fluid saturated velocities and attenuation factors versus frequency and pressure. The predicted frequency dependency is a consequence of using soft porosity with a single aspect ratio. Many experimental studies show a smoother variation of the quality factor with frequency, or even a constant value. In the context of squirt-flow models, such frequency dependency can be explained by assuming a broad distribution of aspect ratios (O'Connell and Budiansky, 1977). This is also invoked to explain the exponential stress dependency of elastic moduli. However, an analysis based on the theory of Shapiro (2003) suggests that such stress dependencies can be explained by a combination of only two aspect ratios: one for stiff pores and one for soft pores (Pervukhina et al., 2010).

In summary, the novelty of this model consists in the following: (1) It is exactly consistent with Gassmann's theory in the low-frequency limit, and with Mavko-Jizba unrelaxed moduli in the high-frequency limit (Mavko and Jizba, 1991). (2) All the parameters of the model have a clear physical meaning. There is only one adjustable parameter: the aspect ratio of compliant pores (grain contacts). All other parameters can be measured or estimated from measurements of ultrasonic velocities and strains versus confining pressure on dry samples (Shapiro, 2003). Since the theory has many parameters, it is always possible to fit the data by varying the unknown parameters. It is therefore critical to be able to measure or estimate independently as many parameters as possible, that is, to perform a controlled experiment. In this model, we use the gap aspect ratio as a free fitting parameter and estimate it as the value that provides the best fit for stiffness-pressure dependency on saturated samples. A workflow for the estimation of these parameters is given in Gurevich et al. (2010). (3) The theory can be implemented exactly in the time domain, without the need of time convolutions.

Regarding the present work, its novelty resides in the following: (a) The squirt-flow wave attenuation mechanism is implemented in Biot's theory of poroelasticity in the form of differential equations, and (b) These equations are solved by using a numerical algorithm based on memory variables. The wavefield is obtained using a grid method based on the Fourier differential operator and a Runge-Kutta time-integration algorithm. Since the presence of the slow quasi-static mode makes the differential equations stiff, a time-splitting integration algorithm is used to solve the stiff part analytically. The modeling is second-order accurate in the time discretization and has spectral accuracy in the calculation of the spatial derivatives (Carcione and Quiroga-Goode, 1995; Carcione, 2007). The algorithm, which allows general material variability, provides snapshots and time histories of the rock-frame and fluid particle velocities, and corresponding stress components.

STRESS-STRAIN RELATIONS INCLUDING THE SQUIRT-FLOW MECHANISM

Stress-strain relations

In the absence of body sources, the time-differentiated stress-strain relations for an inhomogeneous isotropic poroelastic medium, according to Biot's theory are

$$\dot\sigma_{ij} = 2\mu_G d_{ij} + K_G \vartheta \delta_{ij} + \alpha M \varphi \delta_{ij},$$
$$\dot p_f = -M(\varphi + \alpha\vartheta),$$

where $\vartheta \equiv \nabla \cdot \mathbf{v}$, $\varphi \equiv \nabla \cdot \mathbf{q}$, $d_{ij} \equiv \frac{1}{2}(\partial_i v_j + \partial_j v_i) - \frac{1}{3}\delta_{ij}\vartheta$, (2)

(Biot, 1962; Carcione, 2007). Moreover, σ_{ij} are the total stress components, p_f is the phase-averaged pressure fluctuation in the fluid,

v is the phase-averaged particle-velocity vector of the solid constituent of the two-phase poroelastic medium, with components v_i, and **q** is the porosity-weighted relative fluid velocity with respect to the solid. A dot above a variable denotes time differentiation, ∂_i denotes spatial differentiation with respect to the x_i-coordinate, and δ_{ij} is the Kronecker delta. The stress-strain relations are written in the particle-velocity/stress formulation, which is suitable to perform numerical simulations.

The poroelastic coefficients are the Gassmann bulk and shear moduli,

$$K_G = K_m + \alpha(K_m)^2 M(K_m) \quad \text{and} \quad \mu_G = \mu_m \tag{3}$$

and

$$\alpha(K_m) = 1 - \frac{K_m}{K_s} \quad \text{and} \quad M(K_m) = \frac{K_s}{1 - \phi - K_m/K_s + \phi K_s/K_f}, \tag{4}$$

where ϕ is the porosity, K_m and μ_m are the bulk and shear moduli of the drained matrix, and K_s and K_f are the solid and fluid bulk moduli, respectively (e.g., Carcione, 2007). We explicitly indicate the functional form of α and M on K_m because we shall replace this modulus by a modified matrix (or frame) complex modulus K, which includes the squirt-flow mechanism. In the same manner, μ_m will be replaced by μ. The new moduli are complex-valued and frequency dependent.

Squirt-flow model

The squirt-flow model is based on the fact that the pore space of many rocks has a binary structure: relatively stiff pores, which constitute most of the pore space, and relatively compliant (or soft) pores, which are responsible for the pressure dependency of the poroelastic moduli. When the frequency is higher than the squirt characteristic frequency, the fluid pressure does not have enough time to equilibrate between stiff and compliant pores during a half-wave cycle (the so-called unrelaxed state). Then, compliant pores at the grain contacts are effectively isolated from the stiff pores and hence, become stiffer with respect to normal (but not tangential) deformation. To model the frequency dependency of the moduli, Gurevich et al. (2010) assume the geometrical configuration proposed by Murphy et al. (1986): a compliant pore forms a disk-shaped gap between two grains, and its edge opens into a toroidal stiff pore (Figure 1).

Using this model, the bulk and shear moduli of the saturated rock at low frequencies are given by Gassmann's equations,

$$K_G = K + \alpha^2(K) M(K) \quad \text{and} \quad \mu_G = \mu, \tag{5}$$

where K and μ are the bulk and shear moduli of the modified frame including the unrelaxation due to the presence of the squirt-flow mechanism, and α and M are given by equation 4 substituting K_m with K. For simplicity, we keep the same notation for the Gassmann moduli, but now they are complex-valued and frequency dependent.

Gurevich et al. (2009, 2010) obtained the modified dry moduli in the following form:

$$\frac{1}{K} = \frac{1}{K_h} + \left[\left(\frac{1}{K_m} - \frac{1}{K_h}\right)^{-1} + \left(\frac{1}{K_f^*} - \frac{1}{K_s}\right)^{-1} \phi_c^{-1}\right]^{-1},$$
$$\frac{1}{\mu} = \frac{1}{\mu_m} - \frac{4}{15}\left(\frac{1}{K_m} - \frac{1}{K}\right), \tag{6}$$

where K_m and μ_m are the dry-rock bulk and shear moduli at the confining pressure p_c, K_h is the dry-rock bulk modulus at a confining pressure where all the compliant pores are closed, i.e., an hypothetical rock without the soft porosity, and ϕ_c is the compliant porosity. This is so small — nearly 0.001 for most rocks — that the total porosity ϕ can be assumed to be equal to the stiff porosity. The key quantity in equations 6 is the effective bulk modulus of the fluid saturating the soft pores

$$K_f^* = \mathrm{i}\omega\eta^*, \tag{7}$$

where

$$\eta^* = \frac{3}{2}\left(\frac{R}{h}\right)^2 \eta, \tag{8}$$

is an effective viscosity, η is the fluid shear viscosity, R is the radius of the crack and h is its thickness (see Figure 1). This equation has the restriction that the fluid modulus must satisfy

$$K_f \gg 8\phi_c \left(\frac{1}{K_m} - \frac{1}{K_h}\right)^{-1}. \tag{9}$$

This indicates that this modulus should not be too small, i.e., the fluid inside the crack must be a liquid.

An exact expression of the effective fluid modulus obtained by Gurevich et al. (2010), without invoking the condition of equation 9, is

$$K_{f\text{exact}}^* = \left[1 - \frac{2J_1(kR)}{kRJ_0(kR)}\right] K_f, \qquad k = \frac{2}{h}\sqrt{-\frac{3\mathrm{i}\omega\eta}{K_f}} = \frac{1}{R}\sqrt{\frac{-8K_f^*}{K_f}}, \tag{10}$$

where J_0 and J_1 are Bessel functions.

Zener model representations

At this stage, all the coefficients involved in the constitutive equations 2, μ_G, K_G, M, and αM, are real-valued quantities.

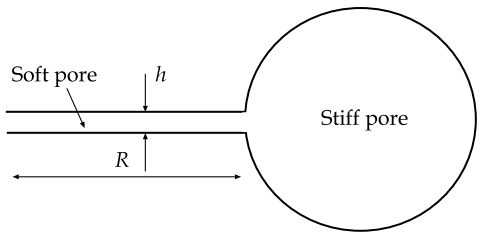

Figure 1. Sketch of the squirt-flow model, where two sandstone grains in contact are shown. The soft pores are the grain contacts and the stiff pores constitute the main porosity. The quantity R is the radius of the disk-shaped soft pore (half disk is represented in the plot).

To include the squirt-flow loss in Biot's equations, we replace K_m by K in these coefficients and express them as complex and frequency-dependent functions in the frequency domain, or relaxation functions in the time domain. We show that these functions can exactly be represented by the Zener mechanical model in all the cases. This fact allows us to perform numerical simulations in the time domain.

The Zener modulus has the form

$$Z = Z(M_R, \tau_\epsilon, \tau_\sigma) = M_R\left(\frac{1+\mathrm{i}\omega\tau_\epsilon}{1+\mathrm{i}\omega\tau_\sigma}\right), \tag{11}$$

where M_R is the relaxed modulus, and τ_ϵ and τ_σ are relaxation times. Equation 11 represents a mechanical model (e.g., Carcione, 2007) made of two springs and a dashpot. A quality factor $Q = \mathrm{Re}(Z)/\mathrm{Im}(Z)$ can be associated with this modulus, whose dissipation factor $1/Q$ is a symmetric relaxation peak as a function of the logarithm of the frequency. The exact location of the relaxation peak is

$$f_0 = \frac{\omega_0}{2\pi}, \qquad \omega_0 = \frac{1}{\sqrt{\tau_\epsilon\tau_\sigma}}. \tag{12}$$

and the minimum value of the quality factor at the peak is

$$Q_0 = 2[\omega_0(\tau_\epsilon - \tau_\sigma)]^{-1}. \tag{13}$$

The relaxation function ψ associated with the modulus of equation 11 is such that

$$Z = \mathcal{F}(\dot{\psi}), \tag{14}$$

where $\mathcal{F}$ is the time Fourier transform and

$$\psi(t) = \psi_0\left(\frac{\tau_\sigma}{\tau_\epsilon}\right)\left[1 + \left(\frac{\tau_\epsilon}{\tau_\sigma} - 1\right)\exp(-t/\tau_\sigma)\right]H(t) \equiv \psi'(t)H(t), \tag{15}$$

where $\psi_0 = M_R\tau_\epsilon/\tau_\sigma$ and H is the Heaviside function.

The Zener equations for the various stiffnesses are then obtained by using equation 6 and replacing K_m with K in equations 3 and 4. We obtain

$$\begin{aligned} K &= Z(K_m, \theta_\epsilon, \theta_\sigma),\\ \mu_G &= \mu = Z(\mu_m, \alpha_\epsilon, \alpha_\sigma),\\ K_G &= Z[K_G(K_m), \beta_\epsilon, \beta_\sigma],\\ M &= Z[M(K_m), \gamma_\epsilon, \gamma_\sigma],\\ \alpha M &= Z[\alpha(K_m)M(K_m), \delta_\epsilon, \delta_\sigma], \end{aligned} \tag{16}$$

where

$$\begin{aligned} \theta_\epsilon &= \frac{\eta^*}{K_s}(a-1), & \theta_\sigma &= \frac{\eta^*}{K_s}\left(\frac{K_m}{K_h}a - 1\right),\\ \alpha_\epsilon &= \theta_\epsilon, & \alpha_\sigma &= \theta_\epsilon - \frac{4\mu_m}{15K_m}(\theta_\epsilon - \theta_\sigma),\\ \beta_\epsilon &= \frac{b\theta_\epsilon + \theta_\sigma}{b+1}, & \beta_\sigma &= \frac{c\theta_\sigma - \theta_\epsilon}{c-1},\\ \gamma_\epsilon &= \theta_\sigma, & \gamma_\sigma &= \beta_\sigma,\\ \delta_\epsilon &= \frac{d\theta_\sigma - \theta_\epsilon}{d-1}, & \delta_\sigma &= \beta_\sigma, \end{aligned} \tag{17}$$

with

$$\begin{aligned} a &= (K_s/\phi_c)(1/K_m - 1/K_h),\\ b &= (f-1)/d,\\ c &= d(f+1),\\ d &= K_s/K_m,\\ f &= \phi(K_s/K_f - 1), \end{aligned} \tag{18}$$

being dimensionless quantities.

Since $K_m \le K_h$, it is $\theta_\sigma \le \theta_\epsilon$, and the dispersion is such that the phase velocity related to modulus K increases with frequency. At zero frequency, the modified frame modulus is equal to the relaxed dry-rock modulus, as expected. At high frequencies, the unrelaxed modulus is $K_m(\theta_\epsilon/\theta_\sigma) = K_m(a-1)/[(K_m/K_h)a - 1)$. Because $\theta_\sigma \le \theta_\epsilon$, it is $\alpha_\sigma \le \alpha_\epsilon$, and the shear modulus μ has the same kind of velocity dispersion.

The peak frequency corresponding to modulus K can be obtained from equations 8, 12, 17, and 18,

$$f_{sf} \approx \frac{K_s}{3\pi\eta a}\left(\frac{h}{R}\right)^2, \tag{19}$$

using the approximations $K_h \approx K_m$ and $a \gg 1$. Hence, the peak frequency decreases with increasing viscosity and decreasing aspect ratio of the crack.

Let us consider the sandstone whose properties are given in Table 1. Condition 12 is satisfied because 2.25 GPa $\gg$ 0.28 GPa.

Table 1. Water-saturated sandstone.

Grain	Bulk modulus, K_s	50 GPa
	Density, ρ_s	2650 kg/m^3
Matrix	Porosity, ϕ	0.2
	Soft porosity, ϕ_c	0.0002
	Bulk modulus, K_m	18 GPa
	Bulk modulus, K_h	20 GPa
	Shear modulus, μ_m	12 GPa
	Grain-contact aspect ratio, h/R	0.0008
	Permeability, κ	200 mD
	Tortuosity, T	2.3
Brine	Bulk modulus, K_f	2.25 GPa
	Density, ρ_f	1040 kg/m^3
	Viscosity, η	1 cP

1 cp = 10^{-3} Pa s; 1 mD $\approx 10^{-15}$ m^2.

We obtain the parameters indicated in Table 2 for the Zener models. The behavior of αM is anomalous because $\delta_\epsilon < \delta_\sigma$, but this fact has no relevance from a physical point of view because the relevant Q-factor is that related to equation 23 and this is always positive.

PHASE VELOCITY AND DISSIPATION FACTOR

In the absence of squirt-flow loss, Biot's theory predicts a relaxation peak. The associated attenuation mechanism has a macroscopic nature. It is the wavelength-scale equilibration between the peaks and troughs of the P-wave. Geertsma and Smit (1961) showed that the dissipation factor $1/Q$ of the fast P-wave, obtained with equation 23 (see below), can be approximated by that of a Zener model for $Q \gtrsim 5$. They obtain the expressions

$$Q^{-1}(\omega) = \frac{\omega(\tau_\epsilon - \tau_\sigma)}{1 + \omega^2 \tau_\epsilon \tau_\sigma}, \quad \tau_\sigma = \left[\frac{v_G}{v_P(\infty)}\right]^2 \tau_\epsilon, \quad \tau_\epsilon = \frac{\mathcal{X}\kappa\rho}{\eta}, \quad (20)$$

where $v_P(\infty)$ is the P-wave phase velocity at the high-frequency limit (e.g., Carcione, 2007; eq. [7.290]), $v_G = v_P(0) = \sqrt{(K_G + 4\mu_G/3)/\rho}$ is Gassmann's velocity, κ is the permeability, $\mathcal{X} = \rho_f \mathcal{T}/(\rho\phi) - (\rho_f/\rho)^2$, $\mathcal{T}$ is the tortuosity of the pore space, $\rho = (1-\phi)\rho_s + \phi\rho_f$ is the bulk density, ρ_s is the grain density and ρ_f is the fluid density.

The location of the Zener relaxation peak is $\omega_B = 1/\sqrt{\tau_\sigma \tau_\epsilon}$. Then, the peak frequency is $f_B = \omega_B/2\pi$ and using equation 20, we get

$$f_B = \left[\frac{v_P(\infty)}{v_G}\right] \frac{\eta}{2\pi\mathcal{X}\kappa\rho} \approx \frac{\eta}{2\pi\mathcal{X}\kappa\rho} = \frac{\phi\eta\rho}{2\pi\kappa\rho_f(\rho\mathcal{T} - \phi\rho_f)}, \quad (21)$$

because Biot's velocity dispersion is rather small. Although Biot's loss mechanism can approximately be represented by a Zener modulus, we model its effects exactly by solving Biot's equations explicitly.

The phase velocity and dissipation factor, including the Biot and squirt-flow mechanisms, are

$$v_P = \left[\mathrm{Re}\left(\frac{1}{v_c}\right)\right]^{-1}, \quad (22)$$

and

$$Q^{-1} = \frac{\mathrm{Im}(v_c^2)}{\mathrm{Re}(v_c^2)} \quad (23)$$

where v_c is the complex velocity (e.g., Carcione, 2007). For shear waves

$$v_c = \sqrt{\frac{\mu_G}{\bar{\rho}}}, \qquad \bar{\rho} = \rho - \rho_f^2/\rho_1 \quad (24)$$

where

$$\rho_1 = \frac{\rho_f \mathcal{T}}{\phi} + \frac{\eta}{\mathrm{i}\omega\kappa}, \quad (25)$$

The complex velocity of the P-waves is obtained from the following second-order equation

$$\bar{\rho}\rho_1 v_c^4 + a_1 v_c^2 + a_0 = 0, \quad (26)$$

where

$$a_1 = (2\alpha\rho_f - \rho)M - \rho_1\left(K_G + \frac{4}{3}\mu_G\right),$$
$$a_0 = \left(K + \frac{4}{3}\mu\right)M \quad (27)$$

(e.g., Carcione, eq. [7.287]).

Figure 2 shows the phase velocities and dissipation factors ($1/Q$) of the fast P-wave and S wave. The solid lines in Figure 2a and 2b correspond to the case including squirt-flow and Biot losses, whereas the dashed line in 2a represents the velocity dependence due to Biot losses only (in this case $v_P(\infty)/v_G = 1.007$). The two relaxation peaks (squirt-flow and Biot) are indicated in the P-wave dissipation factor curve (solid line in Figure 2c). The P-wave peak dissipation factor is approximately equal to 40 at the sonic frequency band. Figure 3 shows the same physical quantities for the slow P-wave. It can be shown that the squirt-flow attenuation mechanism contributes with more slow-wave attenuation, e.g., at 100 Hz, its value is three times the value without squirt-flow loss.

INCORPORATION OF THE SQUIRT-FLOW MECHANISM INTO TIME-DOMAIN BIOT'S EQUATIONS

We implement the squirt-flow mechanism in Biot's poroelastic wave propagation equations by using the well-known concept of memory variables (e.g., Day and Minster, 1984; Carcione et al., 1988). This approach yields a complete, time domain, partial differential formulation of the governing equations which avoids calculation of temporal convolutions.

The complex-valued and frequency-dependent stiffnesses μ_G, K_G, M, and αM, involved in equations 2, transform to time-dependent relaxation functions in the time domain. The products between the poroelastic moduli and field variables are then replaced by time convolutions. In the 3D space/frequency domain, we have the following:

$$\mu_G d_{11}, \quad \mu_G d_{22}, \quad \mu_G d_{33}, \quad \mu_G d_{23}, \quad \mu_G d_{13}, \quad \mu_G d_{12},$$
$$K_G\vartheta, \quad \alpha M\varphi, \quad M\varphi, \quad \alpha M\vartheta, \quad (28)$$

i.e., 10 products, which lead to 10 memory variables. In the time

Table 2. Zener parameters of the stiffnesses.

Modulus	K	μ_G	K_G	M	αM
Relaxation time, τ_ϵ (μs)	65	65	62	58.5	55
Relaxation time, τ_σ (μs)	58.5	64	58	58	58
Peak frequency, f_0 (kHZ)	2.58	2.47	2.65	2.73	2.82
Relaxed modulus, M_R (GPa)	18	12	22	10	6.5
Minimum Q factor, Q_0	19	107	31	260	−39

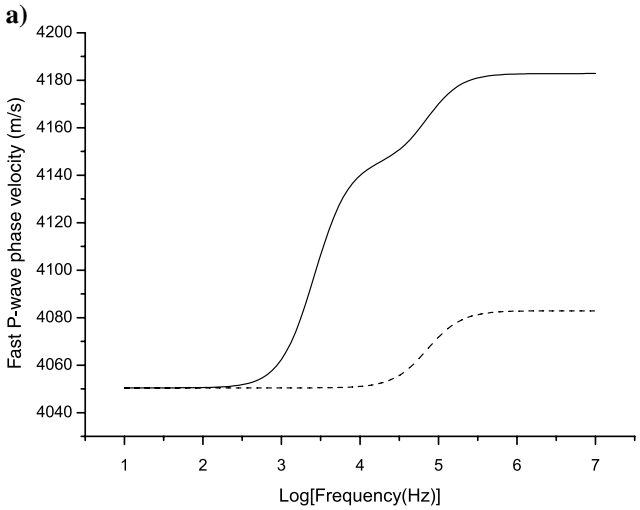

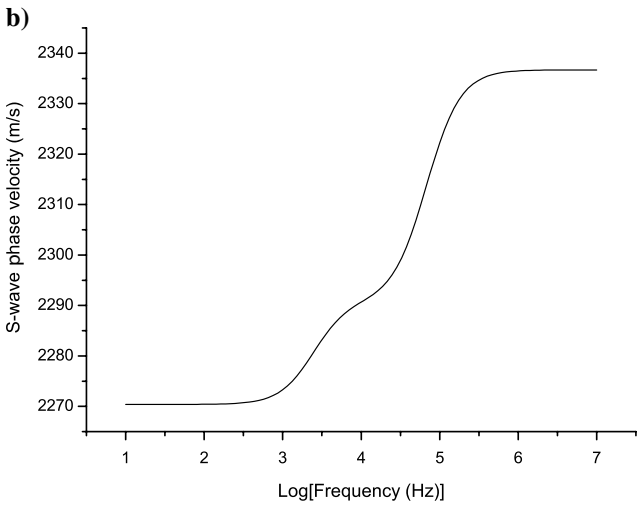

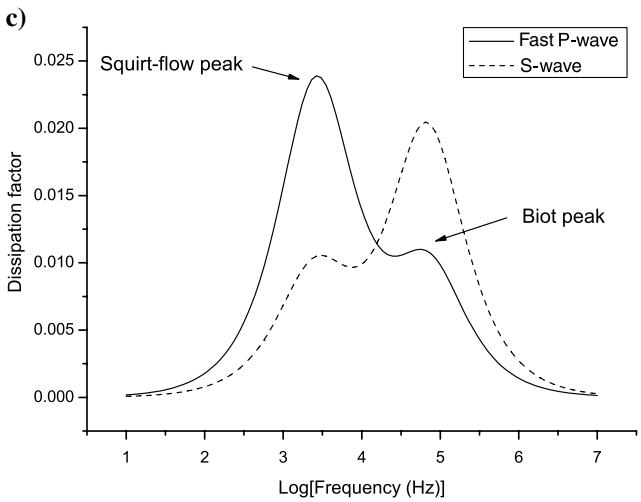

Figure 2. (a) Phase velocity of the fast P-wave, (b) and S-wave , and (c) dissipation factors as a function of frequency. The dashed line in (a) represents the phase velocity without squirt-flow dissipation.

domain, each product is replaced by $\dot{\psi} * u$, where ψ is the associated relaxation function (see equation 15) and u is the field quantity, e.g., $d_{11}, d_{22}, \ldots$, etc. Introducing the memory variable $e = \dot{\psi}' H * u$, the convolution is

$$\dot{\psi} * u = \psi_0 u + e = M_\infty u + e, \qquad M_\infty = \psi_0 = \left(\frac{\tau_\epsilon}{\tau_\sigma}\right) M_R, \tag{29}$$

where

$$\dot{e} = \psi_0 \left(\frac{1}{\tau_\epsilon} - \frac{1}{\tau_\sigma}\right) u - \frac{e}{\tau_\sigma} = \frac{1}{\tau_\sigma}[(M_R - M_\infty)u - e]. \tag{30}$$

We consider the 2D case in the (x, z)-plane. In this case, the formulation leads to seven memory variables, $e_l = 1, \ldots, 7$, associated with the various terms,

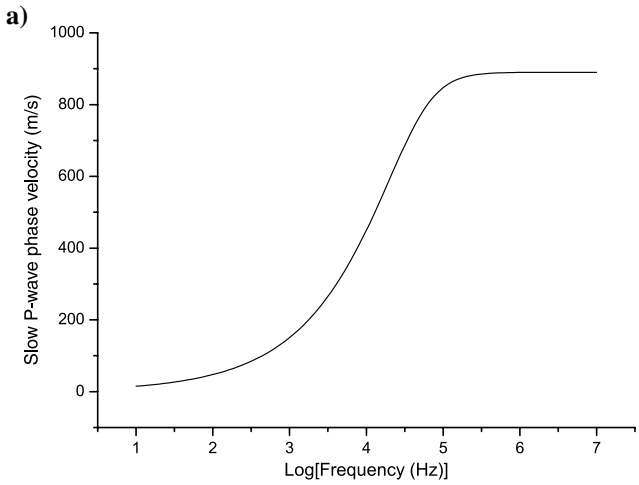

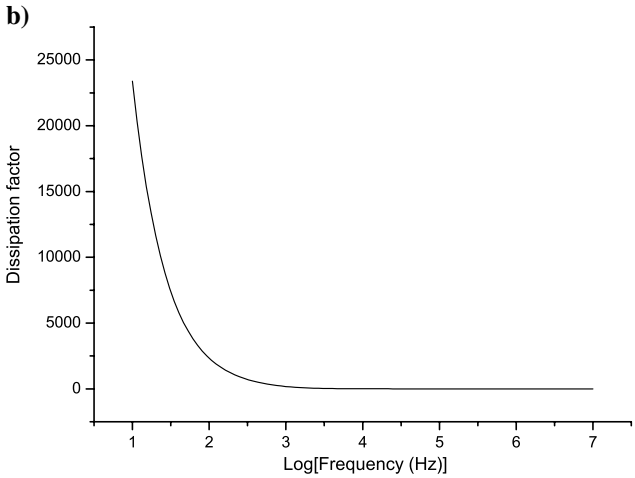

Figure 3. (a) Phase velocity and (b) dissipation factor of the slow P-wave as a function of frequency.

$$
\begin{aligned}
&e_1 \leftrightarrow \mu_G d_{11}, \quad A_1 = \mu_m - \mu_\infty, && u_1 = d_{11}, \quad \tau_1 = \alpha_\sigma,\\
&e_2 \leftrightarrow \mu_G d_{33}, \quad A_2 = \mu_m - \mu_\infty, && u_2 = d_{33}, \quad \tau_2 = \alpha_\sigma,\\
&e_3 \leftrightarrow \mu_G d_{13}, \quad A_3 = \mu_m - \mu_\infty, && u_3 = d_{13}, \quad \tau_3 = \alpha_\sigma,\\
&e_4 \leftrightarrow K_G \vartheta, \quad A_4 = K_G(K_m) - K_{G\infty}, && u_4 = \vartheta, \quad \tau_4 = \beta_\sigma,\\
&e_5 \leftrightarrow \alpha M \varphi, \quad A_5 = \alpha(K_m)M(K_m) - (\alpha M)_\infty, && u_5 = \varphi, \quad \tau_5 = \delta_\sigma,\\
&e_6 \leftrightarrow M\varphi, \quad A_6 = M(K_m) - M_\infty, && u_6 = \varphi, \quad \tau_6 = \gamma_\sigma,\\
&e_7 \leftrightarrow \alpha M \vartheta, \quad A_7 = \alpha(K_m)M(K_m) - (\alpha M)_\infty, && u_7 = \vartheta, \quad \tau_7 = \delta_\sigma, \qquad (31)
\end{aligned}
$$

where

$$
\mu_\infty = \mu_m \frac{\alpha_e}{\alpha_\sigma}, \qquad K_{G\infty} = K_G(K_m)\frac{\beta_e}{\beta_\sigma},
$$
$$
M_\infty = M(K_m)\frac{\gamma_e}{\gamma_\sigma}, \qquad (\alpha M)_\infty = \alpha(K_m)M(K_m)\frac{\delta_e}{\delta_\sigma} \qquad (32)
$$

are unrelaxed moduli, and the A_l, u_l, and τ_l are used below.

The 2D poroelastic equations of motion, including the squirt-flow mechanism, are then

- Biot-Euler's dynamical equations

$$
\begin{aligned}
\partial_1\sigma_{11} + \partial_3\sigma_{13} &= \rho\dot{v}_1 + \rho_f\dot{q}_1,\\
\partial_1\sigma_{13} + \partial_3\sigma_{33} &= \rho\dot{v}_3 + \rho_f\dot{q}_3. \qquad (33)
\end{aligned}
$$

- Dynamical Darcy's law

$$
\begin{aligned}
-\partial_1 p_f &= \rho_f\dot{v}_1 + m\dot{q}_1 + \frac{\eta}{\kappa}q_1,\\
-\partial_3 p_f &= \rho_f\dot{v}_3 + m\dot{q}_3 + \frac{\eta}{\kappa}q_3, \qquad (34)
\end{aligned}
$$

  where $m = \rho_f\mathcal{T}/\phi$.
- Stress-strain relations

$$
\begin{aligned}
\dot{\sigma}_{11} &= 2(\mu_\infty d_{11} + e_1) + K_{G\infty}\vartheta + e_4 + (\alpha M)_\infty\varphi + e_5 + s_{11},\\
\dot{\sigma}_{33} &= 2(\mu_\infty d_{33} + e_2) + K_{G\infty}\vartheta + e_4 + (\alpha M)_\infty\varphi + e_5 + s_{33},\\
\dot{\sigma}_{13} &= 2(\mu_\infty d_{13} + e_3) + s_{13},\\
\dot{p}_f &= -[M_\infty\varphi + e_6 + (\alpha M)_\infty\vartheta + e_7] + s_f, \qquad (35)
\end{aligned}
$$

  where s denotes time-differentiated body moment sources of seismic waves.
- Memory-variable equations

$$
\dot{e}_l = \frac{1}{\tau_l}(A_l u_l - e_l), \qquad l = 1, \ldots, 7, \qquad (36)
$$

  where the u_l are defined in equation 31.

To recast these equations in the particle-velocity/stress formulation, they have to be complemented with the rate of strain/particle-velocity equations,

$$
\begin{aligned}
d_{11} &= \frac{1}{3}(2\partial_1 v_1 - \partial_3 v_3), \quad d_{33} = \frac{1}{3}(2\partial_3 v_3 - \partial_1 v_1),\\
d_{13} &= \frac{1}{2}(\partial_1 v_3 + \partial_3 v_1), \quad \vartheta = \partial_1 v_1 + \partial_3 v_3, \qquad (37)\\
\varphi &= \partial_1 q_1 + \partial_3 q_3.
\end{aligned}
$$

Equations 33–37 contain 15 dependent variables and 16 independent material parameters. The analogous 3D counts are 23 and 16, respectively.

NUMERICAL METHOD

A time-splitting method and a fourth-order Runge-Kutta algorithm are used to solve the differential equations 33, 34, 35, and 36 (Carcione and Quiroga-Goode, 1995; Carcione, 1998, 2007; Carcione et al., 2010). These equations of motion can be recast as $\dot{\mathbf{v}} = \mathbf{M}\cdot\mathbf{v} + \mathbf{s}$, where $\mathbf{v}$ is the vector of unknown variables, $\mathbf{M}$ is the evolution matrix and $\mathbf{s}$ is the source vector. Assume constant material properties and a plane-wave kernel of the form $\exp(\mathrm{i}\mathbf{k}\cdot\mathbf{x} - \mathrm{i}\omega_c t)$, wherein $\mathbf{k}$ is the real wavenumber vector, $\mathbf{x}$ is the position vector and ω_c is a complex frequency. Substitution of the plane-wave kernel into the equation of motion yields an eigenvalue equation for the eigenvalues $\lambda = -\mathrm{i}\omega_c$. The presence of the slow P-wave implies very large negative eigenvalues. Let us denote the discrete time by $t = ndt$, where dt is the time step, and n is a nonnegative integer. Stability of the Runge-Kutta scheme requires $dt|\lambda_{\max}| < 2.79$, where $\lambda_{\max}$ is the largest eigenvalue (Jain, 1984, p. 71). Regarding the Biot loss mechanism, this problem is circumvented by splitting the equations and solving the stiff part analytically. The poroelastic equations can be partitioned into a stiff part and a nonstiff part, such that the evolution operator, involved in the solution of the equation of motion, can be expressed as $\exp(\mathbf{M}t) = \exp(\mathbf{M}_r + \mathbf{M}_s)t$, where r indicates the regular (nonstiff) matrix and s the stiff matrix. The stiff part can be solved analytically and the nonstiff part with the Runge-Kutta method (Carcione and Quiroga-Goode, 1995). Strang's scheme (Jain, 1984) can be shown to be equivalent to the splitting of the evolution operator for solving the poroelastic equations. It remains to consider the eigenvalues corresponding to the Zener mechanisms. These eigenvalues are approximately bounded by the minimum value of $-1/\theta_\sigma$ (Tal-Ezer et al, 1990). Hence, the time step must satisfy $dt \leq 2.79\theta_\sigma$, beside the classical stability relation $dt \lesssim 0.4dx/v_{pm}$, where dx is the maximum grid size and v_{pm} is the maximum fast-P-wave phase velocity.

The spatial derivatives are calculated with the Fourier method, based on uniform, rectangular cells, by using the fast Fourier transform (FFT) (e.g., Carcione, 2007). The Fourier pseudospectral method has spectral accuracy for band-limited signals. Then, the results are not affected by spatial numerical dispersion. Because we use Fourier basis functions to compute the spatial derivatives, equations 33, 34, 35, and 36 satisfy periodic boundary conditions at the edges of the numerical mesh. To avoid wraparound, absorbing strips are implemented at the boundaries of the numerical mesh.

EXAMPLES

We consider the medium defined by Tables 1 and 2, where the grain bulk modulus corresponds to a mixture of quartz and calcite, mainly quartz. The medium is discretized with a mesh of 231×231

points and a grid spacing of 5 cm. A point seismic energy source imparts compressional and shear motion to the poroelastic medium ($s_{11} = s_{33} = s_f = s_{13}$), with the time variation of a Ricker wavelet with peak frequency f_p. The wavefield is computed with a time step of 5 μs, which corresponds to the stability limit. Figure 4a and 4b compare σ_{33} snapshots for $f_p = 3$ kHz and $f_p = 10$ kHz, respectively. Strong velocity dispersion can be observed in agreement with the predictions in Figure 2a and 2b. The slow wave is evident at the source location in Figure 4a, whereas it is not visible in Figure 4b. The attenuation factor is approximately proportional to the frequency times the dissipation factor. Therefore, the higher the frequency the higher the attenuation for a nearly constant quality factor. The calculations indicate that the attenuation factor is six times higher at 10 khz. Figure 5 shows microseismograms of the v_3-component at 4.95 m from a point compressional source ($s_{11} = s_{33} = \phi s_f$, $s_{13} = 0$) (i.e., no shear motion) applied to the solid and fluid phases. The peak frequency is $f_p = 3$ kHz and

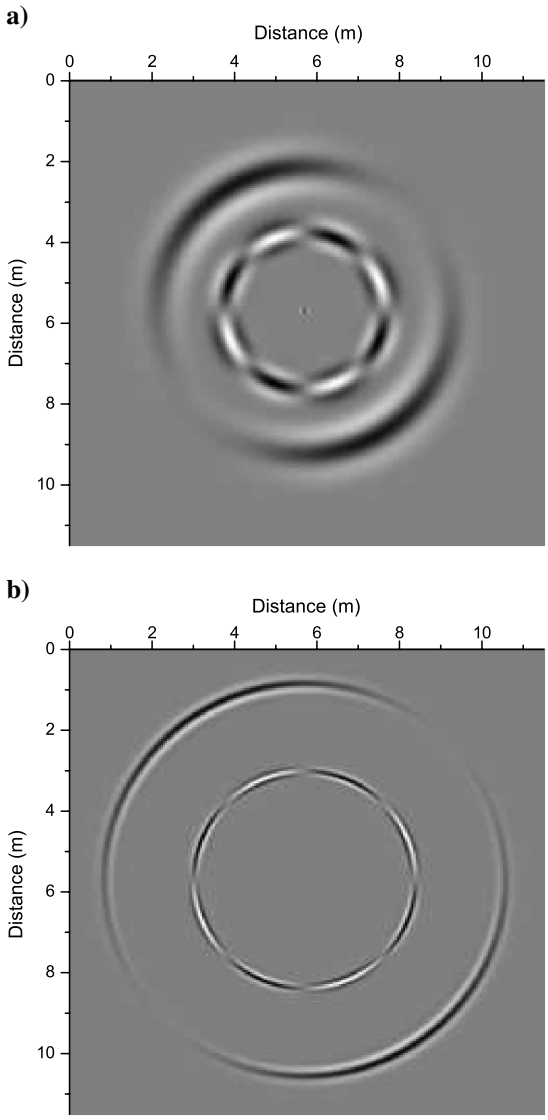

Figure 4. Snapshot at 1.3 ms of the stress component σ_{33} for source peak frequencies of (a) 3 kHz and (b) 10 kHz.

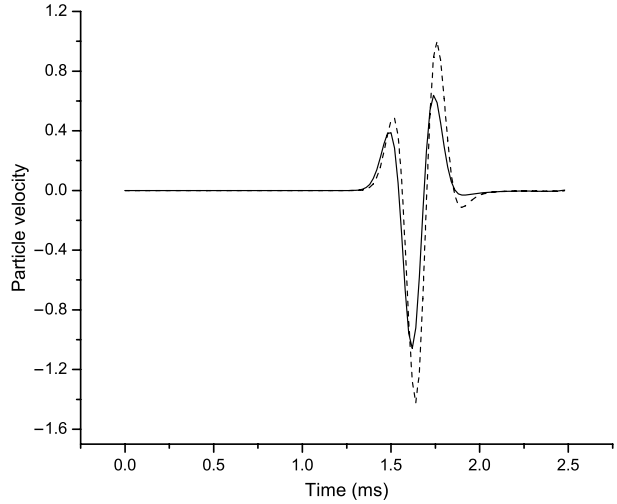

Figure 5. Particle-velocity component v_3 at $(x, z) = (3.5, 3.5)$ m from the source location, with and without the squirt-flow loss mechanism (solid and dashed lines, respectively). The fluid is brine.

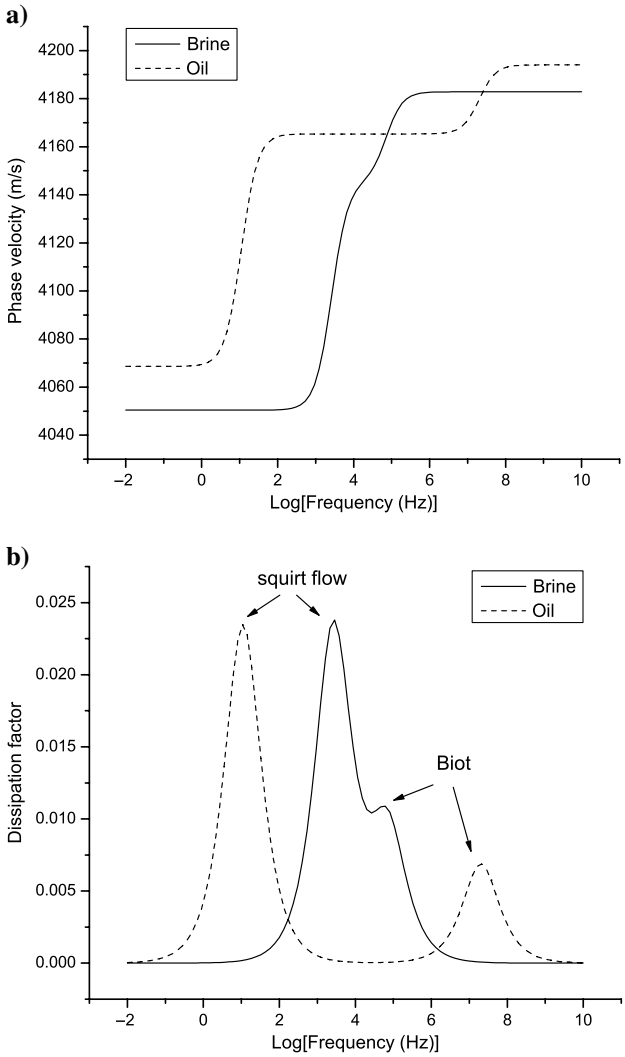

Figure 6. (a) Phase velocity of the fast P-wave and (b) dissipation factors as a function of frequency, corresponding to brine and oil.

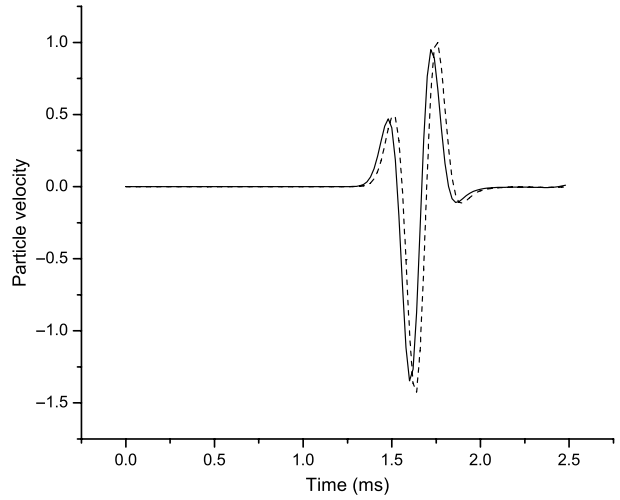

Figure 7. Particle-velocity component v_3 at $(x, z) = (3.5, 3.5)$ m from the source location, with and without the squirt-flow loss mechanism (solid and dashed lines, respectively). The fluid is oil.

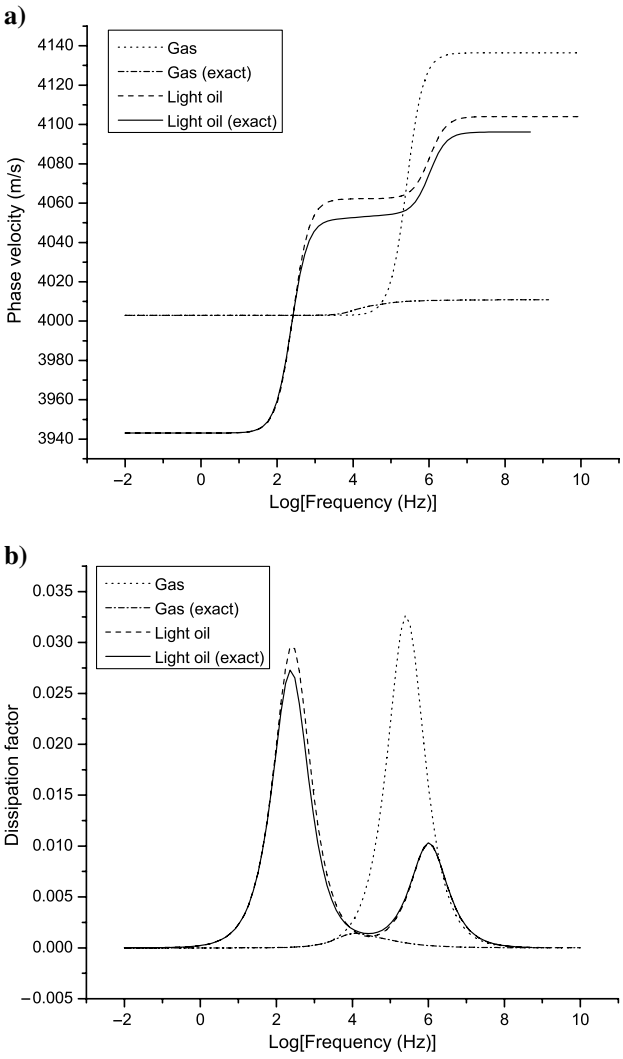

Figure 8. (a) Phase velocity of the fast P-wave and (b) dissipation factors as a function of frequency, corresponding to light oil and gas.

the signal observed in the trace is the P-wave, with the dashed line corresponding to the case without the squirt-flow mechanism. As can be seen, the signal with squirt-flow dissipation arrives earlier, in agreement with Figure 2a.

In the next example, we consider the same matrix but saturated with oil ($K_f = 2.16$ GPa, $\rho = 890$ kg/m^3, and $\eta = 240$ cP). Figure 6 compares the velocity and dissipation factors for brine and oil saturation. As can be seen, for increasing viscosity the squirt-flow peak moves to the lower frequencies unlike the Biot peak, whose shift is toward the high frequencies. The situation is such that the oil-saturated medium absorbs negligible P-wave energy at the sonic band. The same happens with the S-wave. Figure 7 shows v_3 microseismograms from a fluid source with 3 kHz peak frequency. The attenuation is small and slight velocity dispersion can be observed as shown in Figure 6a.

If we consider more compressible fluids for which the approximation 9 is not valid, we observe the behavior shown in Figure 8, where the P-wave phase velocities and dissipation factors of light oil and gas are displayed. The solid and dash-dotted lines correspond to the exact case, using equation 10. Light oil has $K_f = 0.57$ GPa, $\rho = 700$ kg/m^3 and $\eta = 10$ cP, and gas has $K_f = 0.0022$ GPa, $\rho = 10.8$ kg/m^3, and $\eta = 0.001$ cP. For the considered soft porosity, equation 7 is a good approximation for light oil whereas it fails for gas, but in this case, the medium is practically lossless because Q is above 700. If we consider a depth of 3.5 km, the gas bulk modulus is of the order of 0.01 GPa. In this case, the minimum quality factor is nearly 200. Thus, in these cases, we can safely use Biot's equations with zero viscosity in gas-saturated regions. The same remarks hold for the S-wave. However, if the bulk modulus of the fluid is of the order of 0.1 GPa, the minimum quality factor is less than 100 and the approximation becomes less accurate.

CONCLUSIONS

We have designed a space-time domain numerical modeling method to solve the differential equations corresponding to Biot's theory of wave propagation including the squirt-flow loss mechanism. The theory contains one adjustable parameter: aspect ratio of compliant pores (grain contacts). All other parameters can be measured or estimated from measurements of ultrasonic velocities and strains versus differential pressure on dry samples, such as the dry-rock bulk modulus at high confining pressures. The memory-variable approach, used in viscoelasticity as a phenomenological model of attenuation and velocity dispersion, allows us to obtain an exact time-domain fully differential formulation of the equations of motion when the pores are saturated by a liquid. The formulation requires 10 memory variables in 3D space and seven in 2D space. In the presence of gas, we may safely assume lossless propagation, and we can set the fluid viscosity equal to zero to model wave propagation in a gas-saturated medium.

ACKNOWLEDGMENTS

Boris Gurevich acknowledges the financial support of the Australian Research Council (Discovery-Project DP1096232) and the sponsors of Curtin Reservoir Geophysics Consortium (CRGC). The authors thank Dina Makarynska for useful advice. We are grateful to two reviewers and the associate editor for a very meticulous and detailed review.

REFERENCES

Arntsen, B., and J. M. Carcione, 2001, Numerical simulation of the Biot slow wave in water-saturated Nivelsteiner sandstone: Geophysics, **66**, 890–896, doi: 10.1190/1.1444978.

Biot, M. A., 1962, Mechanics of deformation and acoustic propagation in porous media: Journal of Applied Physics, **33**, 1482–1498, doi: 10.1063/1.1728759.

Carcione, J. M., 1998, Viscoelastic effective rheologies for modeling wave propagation in porous media: Geophysical Prospecting, **46**, 249–270, doi: 10.1046/j.1365-2478.1998.00087.x.

Carcione, J. M., 2007, Wave fields in real media: Theory and numerical simulation of wave propagation in anisotropic, anelastic, porous and electromagnetic media (2nd ed.), revised and extended: Elsevier Science.

Carcione, J. M., and H. B. Helle, 1999, Numerical solution of the poroviscoelastic wave equation on a staggered mesh: Journal of Computational Physics, **154**, 520–527, doi: 10.1006/jcph.1999.6321.

Carcione, J. M., D. Kosloff, and R. Kosloff, 1988, Viscoacoustic wave propagation simulation in the earth: Geophysics, **53**, 769–777, doi: 10.1190/1.1442512.

Carcione, J. M., C. Morency, and J. E. Santos, 2010, Computational poroelasticity — A review: Geophysics, **75**, no. 5 A229–A243, doi: 10.1190/1.3474602.

Carcione, J. M., S. Picotti, D. Gei, and G. Rossi, 2006, Physics and seismic modeling for monitoring CO_2 storage: Pure and Applied Geophysics, **163**, 175–207, doi: 10.1007/s00024-005-0002-1.

Carcione, J. M., and G. Quiroga-Goode, 1995, Some aspects of the physics and numerical modeling of Biot compressional waves: Journal of Computational Acoustics, **3**, 261–280, doi: 10.1142/S0218396X95000136.

Chapman, M., S. V. Zatsepin, and S. Crampin, 2002, Derivation of a microstructural poroelastic model: Geophysical Journal International, **151**, 427–451, doi: 10.1046/j.1365-246X.2002.01769.x.

Day, S. M., and J. B. Minster, 1984, Numerical simulation of attenuated wavefields using a Padé approximant method: Geophysical Journal of the Royal Astronomical Society, **78**, 105–118.

Geertsma, J., and D. C. Smit, 1961, Some aspects of elastic wave propagation in fluid-saturated porous solids: Geophysics, **26**, 169–181, doi: 10.1190/1.1438855.

Gurevich, B., and S. L. Lopatnikov, 1995, Velocity and attenuation of elastic waves in finely layered porous rocks: Geophysical Journal International, **121**, 933–947, doi: 10.1111/gji.1995.121.issue-3.

Gurevich, B., D. Makarynska, and M. Pervukhina, 2009, Ultrasonic moduli for fluid-saturated rocks: Mavko-Jizba relations rederived and generalized: Geophysics, **74**, no. 4, N25–N30, doi: 10.1190/1.3123802.

Gurevich, B., D. Makarynska, M. Pervukhina, and O. De Paula, 2010, A simple model for squirt-flow dispersion and attenuation in fluid-saturated granular rocks: Geophysics, **75**, no. 6, N109–N120, doi: 10.1190/1.3509782.

Jain, M. K., 1984, Numerical solutions of differential equations: Wiley Eastern Ltd.

Johnson, D. L., 2001, Theory of frequency dependent acoustics in patchy saturated porous media: Journal of the Acoustical Society of America, **110**, 682–694, doi: 10.1121/1.1381021.

Jones, T. D., 1986, Pore fluids and frequency-dependent wave propagation in rocks: Geophysics, **51**, 1939–1953, doi: 10.1190/1.1442050.

Klimentos, T., and C. McCann, 1988, Why is the Biot slow compressional wave not observed in real rocks?: Geophysics, **53**, 1605–1609, doi: 10.1190/1.1442443.

Masson, Y. J., and S. R. Pride, 2007, Poroelastic finite difference modeling of seismic attenuation and dispersion due to mesoscopic-scale heterogeneity: Journal of Geophysical Research, **112**, B03204, doi: 10.1029/2006JB004592.

Mavko, G., and D. Jizba, 1991, Estimating grain-scale fluid effects on velocity dispersion in rocks: Geophysics, **56**, 1940–1949, doi: 10.1190/1.1443005.

Mavko, G., and A. Nur, 1975, Melt squirt in the aesthenosphere: Journal of Geophysical Research Solid Earth: JGR, **80**, no. 11, 1444–1448, doi: 10.1029/JB080i011p01444.

Müller, T. M., B. Gurevich, and M. Lebedev, 2010, Seismic wave attenuation and dispersion due to wave-induced flow in porous rocks — A review: Geophysics, **75**, no. 5 A147–A164, doi: 10.1190/1.3463417.

Murphy, W. F. I., K. W. Winkler, and R. L. Kleinberg, 1986, Acoustic relaxation in sedimentary rocks: Dependence on grain contacts and fluid saturation: Geophysics, **51**, 757–766, doi: 10.1190/1.1442128.

Norris, A. N., 1993, Low-frequency dispersion and attenuation in partially saturated rocks: Journal of the Acoustical Society of America, **94**, 359–370, doi: 10.1121/1.407101.

O'Connell, R. J., and B. Budiansky, 1977, Viscoelastic properties of fluid-saturated cracked solids: Journal of Geophysical Research, **82**, 5719–5735, doi: 10.1029/JB082i036p05719.

Pervukhina, M., B. Gurevich, D. N. Dewhurst, and A. F. Siggins, 2010, Applicability of velocity–stress relationships based on the dual porosity concept to isotropic porous rocks: Geophysical Journal International, **181**, 1473–1479, doi: 10.1111/j.1365-246X.2010.04535.x.

Pride, S. R., J. G. Berryman, and J. M. Harris, 2004, Seismic attenuation due to wave induced flow: Journal of Geophysical Research, **109**, B01201, doi: 10.1029/2003JB002639.

Rubino, J. G., J. E. Santos, S. Picotti, and J. M. Carcione, 2007, Simulation of upscaling effects due to wave-induced fluid flow in Biot media using the finite-element method: Journal of Applied Geophysics, **62**, 193–203, doi: 10.1016/j.jappgeo.2006.11.003.

Shapiro, S. A., 2003, Elastic piezosensitivity of porous and fractured rocks: Geophysics, **68**, 482–486, doi: 10.1190/1.1567216.

Tal-Ezer, H., J. M. Carcione, and D. Kosloff, 1990, An accurate and efficient scheme for wave propagation in linear viscoelastic media: Geophysics, **55**, 1366–1379, doi: 10.1190/1.1442784.

Toms, J., T. M. Müller, R. Ciz, and B. Gurevich, 2006, Comparative review of theoretical models for elastic wave attenuation and dispersion in partially saturated rocks: Soil Dynamics and Earthquake Engineering, **26**, 548–565, doi: 10.1016/j.soildyn.2006.01.008.

White, J. E., 1975, Computed seismic speeds and attenuation in rocks with partial gas saturation: Geophysics, **40**, 224–232, doi: 10.1190/1.1440520.

White, J. E., N. G. Mikhaylova, and F. M. Lyakhovitskiy, 1976, Low-frequency seismic waves in fluid-saturated layered rocks: Physics of the Solid Earth, **11**, 654–659.

Zener, C., 1948, Elasticity and anelasticity of metals: University of Chicago Press.